EXPERIMENTAL INVESTIGATION OF DEPOSITION OF CRUDE OIL COMPONENTS IN BRINE-FILLED PORES

Andrew Fogden
Applied Mathematics, Australian National University, Canberra, Australia

This paper was prepared for presentation at the International Symposium of the Society of Core Analysts held in Noordwijk, The Netherlands 27-30 September, 2009

ABSTRACT

It is often presumed that fine-scale surface pores and roughness in reservoir rock remain water-wet. To test this assumption, deposition tendency of asphaltenes and resins during crude oil aging of brine-filled pores was investigated. Model frameworks of water-wet silica with sub-micron pores were synthesized as planar films of thickness 5 μm. These pore networks were conditioned in brine, submerged wet into crude oil for aging in the absence of applied pressure, then cleaned. Brines covering a wide range of NaCl concentrations, without or with added $CaCl_2$ and/or brine degassing, were analyzed. Spectroscopy and microscopy were employed to determine the amount and distribution of asphaltene/resin deposits. The results clearly demonstrate that crude oil is capable of spontaneously invading these fine pores to render them oil-wet. All samples exhibited at least some deposition, with the overall NaCl concentration having little effect, whereas the increasing presence of $CaCl_2$ led to a reduction in deposition. Scanning electron microscopy revealed that deposition typically took the form of uniform thin layers lining pore walls. A mechanism for spontaneous displacement of brine from tight water-wet pores, based on local rupture of convexly-curved brine thin films, is discussed.

INTRODUCTION

Reservoir wettability is largely dictated by the ability/inability of the more polar heavy components of the crude oil, namely its asphaltenes and resins, to adsorb or deposit over geological timescales on rock pore surfaces to alter their originally water-wet state. This depends on rock mineralogy and surface properties, oil and connate brine composition and their temperature and pressure history of pore occupation. The most widely accepted model, termed mixed wettability [1-6], predicts that pore surfaces supporting sufficiently high local meniscus curvature to prohibit displacement at the maximum applied capillary pressure of primary drainage remain overlain by their bulk brine and retain water-wetness. Surfaces presenting lower curvature can admit oil and be altered to oil-wet if directly exposed via rupture of the intervening thin brine film. Special core analysis attempts to reproduce the wettability state in the reservoir through cleaning, reinstating the brine and draining with the crude oil and aging at reservoir conditions. Subsequent displacement testing yields global empirical wettability measures such as Amott-Harvey index [3] or rates and extents of recovery by spontaneous brine imbibition [7]. Analogous brine-oil aging treatments are applied to flat smooth mineral substrates (e.g. glass, quartz, mica, calcite) to measure contact angle behavior [8] and nanoscale morphology of adsorbed or deposited layers by AFM [9], in order to interpret core analysis results or aid in simulating them by network modeling [10].

Despite the developments in techniques for 3D pore-scale structural characterization of rock cores, direct methods to map the distribution of local wettability borne by the pore walls remain elusive. This knowledge gap limits applicability of wettability studies on smooth impervious substrates, in turn limiting the predictive power of simulations of multiphase transport. One means to bridge this gap is to introduce greater complexity, in particular capillarity, to these model substrates, i.e. as new classes of micromodels facilitating direct analysis of their true wettability state. To start with, rock grains, their cements and microscopic particle aggregates lining them present rough and possibly microporous surfaces to the fluids. During primary drainage it could be expected that the connate brine remains held in these tightly curved features, accentuating water wetness and connectivity. The current study directly probes this assumption by utilizing recent advances in materials chemistry which provide simple approaches to synthesis of inorganic pore frameworks with well-controlled sub-micron pores [11-12]. Porous silica films are prepared, brine-oil treated and their oil deposition tendencies analyzed.

PROCEDURES

Preparation of porous silica films

Tetraethylorthosilicate (TEOS) was used as silica precursor and one of two commercial styrene-butadiene latex products, HPS 59 or HPS 61 (Dow Chemical), acted as the organic template. The latex particles are highly spherical and monodisperse, with average size 140 and 130 nm for HPS 59 and HPS 61, delivered as aqueous dispersions at concentrations of approx. 50 wt%. The styrene/butadiene ratio for HPS 59 is lower, leading to a lower glass transition temperature, T_g, of 8^{o}C compared to 26^{o}C for HPS 61. TEOS was pre-hydrolyzed by adding 2.0 g of it to 2.8 g of 0.24 M HCl under strong stirring, leading to a clear sol after 12 min. An amount of 2.4 g of this sol was added to 2.88 g of the latex dispersion under stirring, with 2 pipette drops of the homogeneous mixture then spread as uniformly as possible over an area 56.5 mm x 25.5 mm on each of 12 clean microscope glass slides. The wet film dries under ambient conditions within approx. 1 min, yielding a transparent film in the case of HPS 59, with T_g below room temperature (21^{o}C), and a translucent semi-opaque film with HPS 61, as its higher T_g inhibits latex particle coalescence. Samples were left for 6 days to enhance condensation of the silica framework and diffusion to the top surface of surfactant (from the latex dispersion) remaining mobile in the film. The slides were immersed in deionized water (Millipore Milli-Q) at 35^{o}C for 5 min. to dissolve the free surfactant, dried and then calcined in an air oven (ramped from 21^{o}C to 550^{o}C over 4 h., held at this level for 8 h., then cooled to 21^{o}C over 8 h.) to remove the latex template from the film to leave the silica framework. For both latex types all silica film samples were very strongly bonded to their glass substrates. Films templated by the softer latex, HPS 59, were transparent, while those for HPS 61 were somewhat less so and with slightly more heterogeneity.

Brine-crude oil treatment

The 12 film-covered slides for each latex type were scored and snapped across their length into rectangular pieces of width 14-16 mm. Each piece was immersed in water to dissolve any residual salt in the silica framework, followed by an ethanol bath, and dried by nitrogen blowing. Plasma cleaning was then performed using an in-house RF water-plasma treatment unit, operated at 100 W for 30s, to vaporize any residual organic trace contaminants and restore hydroxyl groups to the framework walls [13]. Each slide piece was directly immersed in 20 ml of its chosen brine in a capped glass vial to equilibrate for 3 h. A matrix of 12 such brines was addressed, comprising aqueous solutions of

NaCl at the 6 concentrations of 16, 32, 64, 128, 256, 512 mM, without or with 10% (mol/mol) added $CaCl_2$ (i.e. ranging from 1.6 to 51.2 mM). The pH values of these 12 solutions were clustered around 5.8, as expected for Milli-Q water in equilibrium with dissolved carbon dioxide and oxygen. For the three highest concentrations in both series the experiments were repeated with the 3 h. immersion period followed by transfer of the brine with its submerged slide piece to an in-house degassing set-up for 20 min. of nitrogen sparging to remove CO_2 and O_2. The corresponding pH values were close to neutral for the NaCl brines and somewhat lower (approx. 6.3) with added $CaCl_2$.

The crude oil used was from the Minnelusa field, with density 0.9039 g/cm^3, refractive index 1.5201, viscosity 58.1 cP, n-C_7 asphaltene content 7.2 wt%, and acid and base numbers 0.12 and 1.71 mg KOH/g [Buckley, private communication]. Each slide piece was immediately transferred from its brine, while remaining wet, to a capped glass jar containing approx. 15 ml of oil, with the oil height more than sufficient to submerge the standing piece. Each jar was placed in an air oven at 60^{o}C to age in the dark for 72 h. The piece was removed with its adhering oil and directly immersed in 20 ml of decalin (decahydronaphthalene) for 5 min. to dissolve and remove the non-adsorbed/deposited crude oil components from the silica framework. It was then transferred to a second fresh decalin bath for 8 h., followed by 8 h. in 20 ml of heptane to remove residual maltene components, then blown dry with nitrogen. Finally it was immersed in 20 ml of water to dissolve residual salt from the brine, then dried again. The brownness of each piece due to any deposition did not noticeably change after removal from the first decalin bath. All samples were stored in the dark during and after these cleaning steps.

To provide spectroscopic calibration standards to quantify asphaltene amount residing in the framework of these samples, the asphaltene fraction of the Minnelusa crude was sedimented by adding 1 ml oil to 39 ml heptane and collected by decanting the maltene fraction and ambiently drying the sediment. This asphaltene yield was dissolved in toluene to provide a stock solution of concentration 0.229 wt%, subsequently diluted by factors of 125, 166.7, 250, 333.3, 500, 666.7, 1000 and 2000 to provide 8 standards for solution-phase calibration. Dry-phase calibration standards were made using a 50 times dilution of the stock solution and an originally clean porous silica film piece for the two latex types. This solution was pipetted onto the porous side of the slide piece to cover its area, dried ambiently to evaporate the toluene, repeated three times, and then analyzed (see below). This four-step process of progressively increasing asphaltene mass (known by weighing the transferred solution) dried in the silica framework was repeated 7 times on this same piece, with analysis following each series. This gradual increase in asphaltene loading from dilute solution was employed to ensure uniformity of its distribution upon drying by avoiding accumulation in bands at the drying front.

Analysis of porous silica films

All brine-oil treated film slide pieces, untreated clean counterparts of the two latex types, and their dry-phase calibration standard series were analyzed using a UV-visible scanning spectrophotometer (Shimatzu UV-3101PC), with the slide lightly clamped in its sample holder perpendicular to the incident beam, porous film side facing forwards, with a clean microscope glass slide in the reference holder. Transmission spectra were recorded with a 1 nm slit width over the interval 800-300 nm, with 6 spectra obtained per sample piece by translating it to obtain an average over the full central area.

Solution-phase calibrations used quartz cells of 50 mm path length and 10 mm width, with the asphaltene standard solution in the sample cell and toluene in the reference cell. Following this, the brine-oil treated sample pieces were imaged by document scanner (Konica Minolta C252), with the full matrix of 18 samples for each latex type imaged simultaneously, and with film side facing the glass and white paper covering the back side. From the 600 dpi jpeg scanned image, smaller images for each piece were cropped and the statistics of their pixel color distributions, reflecting the deposited asphaltenes, were extracted using ImageJ software for comparison with spectroscopy results.

The latex-templated silica framework films on their slides were imaged using a field emission scanning electron microscope (FESEM, Zeiss UltraPlus Analytical) under high vacuum in secondary electron mode at 1 kV. All samples were lightly sputter-coated with platinum to a thickness of approx. 1 nm to minimize beam charging. Corresponding samples after brine-oil treatment were also imaged in the same way, after all other analyses mentioned above had been performed.

RESULTS

Properties of porous silica films

Figure 1 displays the local microstructure of the silica frameworks produced by the two latex types. Both latexes dry to form domains with approximately face-centered cubic (fcc) sphere packing and with the hydrolyzed TEOS progressively condensing to an amorphous gel filling the interstices. The softer latex (HPS 59) partially coalesces with its neighbors, enlarging and flattening the contact zones from which the polymerizing silica precursors are expelled. On calcination the pores vacated by latex are thus more polyhedral for HPS 59, the circular throats joining them are larger, and the framework of amorphous silica is more strut-like. From analysis of FESEM surface images the average in-plane cell repeat distance for HPS 59 and HPS 61 is 151 and 126 nm, and highly monodisperse, largely reflecting the latex sphere sizes. From lower resolution images the harder latex exhibits a smaller ordered domain size and more film cracks on larger length scales, giving its lower transparency. Coat weights of the films on glass before and after calcination, from measured mass difference per known application area, are listed in Table 1 (along with their mass ratio) as mean and standard deviation over the 12 slide samples of the two types, and exhibit good reproducibility given the manual coating. Table 1 also provides the corresponding statistics of film thickness and porosity inferred from the component densities. Full conversion of TEOS to SiO_2 implies a mass ratio of 0.167, somewhat higher than the measured values due to a combination of moisture retention in the uncalcined film and loss of poorly polymerized or bound silica in the water bath to remove surfactant, especially likely for the incompletely film-formed latex HPS 61. The average film thickness after calcination would correspond to around 44 and 55 stacks of pores for HPS 59 and HPS 61 for a defect-free fcc packing.

Scanning of brine-oil treated states

The porous silica films are a useful complement to the smooth impervious substrates (e.g. bare microscope glass) usually employed to analyze crude oil deposits. In addition to their relevance to brine-filled fine rock pores and surface roughness, a thin asphaltene layer undetectable visually or by UV-visible spectroscopy has its signal amplified around 100 fold by the transparent multiple pore stacks bearing this layer on their walls. It is directly apparent to the naked eye that all sample slide pieces in this study, after oil treatment, post-cleaning and drying, exhibit at least some degree of residual brownness

signifying asphaltene deposition. A document scanner is thus a simple, convenient means to visualize trends. Figure 2 provides the full set of scanned images cropped to rectangular areas of height approx. 22 mm and width 10-12 mm, i.e. not sampling the approx. 2 mm bordering all irregularly cut edges, and oriented as they stood in the oil. The brownness distribution is reasonably uniform, with some variations such as vertical stripes directly reflecting variations in local porous silica film thickness from coating. The number affixed to each image is its average gray scale value (GSV), with 0 and 255 signifying totally black and white. The trends are quantitatively identical regardless of whether GSV or division into red, green and blue channels is considered. For the HPS 59-templated porous silica films, oil deposition decreases (GSV increases) slightly to reach a plateau with increasing NaCl brine concentration. The added presence of 10% (mol/mol) $CaCl_2$ generally suppresses deposition to some degree, especially at the highest concentrations. For the HPS 61 counterparts the behavior is roughly similar, with little change in deposited amount across the pure NaCl brines, and with increasing calcium addition reducing deposition to exhibit monotonically increasing GSV for this mixed salt series. Brine degassing prior to oil exposure appears to have some effect, acting to increase deposition for pure NaCl while generally exhibiting the reverse tendency for the NaCl-$CaCl_2$ brines. Thus high calcium contents, possibly accompanied by degassing, are the most effective brine conditions for hindering deposition.

UV-visible spectroscopy

This technique provides similar information to the scanner, but allows more scientific and quantitative spectral analysis. Figure 3 displays the spectrum of transmittance T (percentage ratio of transmitted to incident light intensity, relative to an uncoated glass slide) averaged over 6 subareas per porous silica film-coated slide piece a) in the clean state, sampling 2 and 3 such pieces for HPS 59 and HPS 61, b) the first of the 8 dry-state calibrations with lowest known amount of asphaltene deposited from solution, or c) after oil treatment and post-cleaning for each of the 6 calcium-containing brines. At high wavelengths the transmittance of the HPS 59-templated film is close to 100%, and gradually drops for both types as wavelength decreases towards the film pore size range, maintaining an almost constant difference of 30 percentage units (p.u.) between the two curves. Variations across different pieces and locations on the same piece are relatively slight, with standard deviation (error bars in Figure 3) averaging approx. 2 p.u.

The reduction in transmittance for the dry-state calibration curves (dashed in Figure 3) due to brownness of the deposited asphaltenes strengthens at lower wavelengths. The relative transmittance T_r, i.e. ratio between T for deposited and clean states, decreases with wavelength due to heightened asphaltene absorption in the UV-blue interval as expected [14]. Thus for the set of 6 spectra in Figure 3 after brine-oil treatment, the lower wavelengths will be most sensitive to differences in deposited asphaltene amount. For HPS 59 the hierarchy of these 6 curves is largely independent of wavelength, but amplified at the lower end, while for HPS 61 only these lower wavelengths convey reliable deposition information due to variations in porous film transparency at the high end. For these reasons 365 nm in the UVA interval is chosen for deposition quantification. This choice is further justified by the upper diagram in Figure 4, which compares the average relative transmittance at the two wavelengths of 365 nm and 550 nm (green light) with the average GSV from scanning for the full sample matrix in Figure 2. At the lower wavelength (filled symbols) the results of the two techniques are strongly correlated, while at 550 nm the correlation only holds for the HPS 59 type.

Calibration

Consider first the traditional solution-phase calibration using the above-mentioned 8 dilute solutions of asphaltene in toluene. The Beer-Lambert law predicts that the light absorbance *A* of the solute, i.e. the negative logarithm of the relative transmittance, is linearly related to the solute volume *v* encountered per cross-sectional area *a* as:

$$A = -\log_{10} T_r = \varepsilon' \frac{v}{a} \quad (1)$$

where the constant ε' is the molecular absorptivity density. The measured absorbance at 365 nm of the 8 solutions indeed yields this linear relation to very high accuracy (graph not shown), and assuming asphaltene density as 1.18 g/cm^3, the slope $\varepsilon' = 2.4232\ \mu m^{-1}$. For the 8 dry-phase calibration standards for the HPS 59 and HPS 61 porous film types, measured absorbance *A* at 365 nm and the corresponding values of *v/a*, obtained from the known solution concentration and measured mass applied over the known slide piece area, are plotted in the lower two images of Figure 4. The linear fit (gray lines in Figure 4) to the first 3 measured points verifies that equation 1 remains valid for low asphaltene loadings in the porous framework, and with slope very similar to the ε' value inferred above. At higher loadings saturation effects enter, causing the absorbance to dip increasingly below the linear fit. The augmented Beer-Lambert equation:

$$A = -\log_{10} T_r = \varepsilon' \frac{v}{a} \Big/ \left(1 + \beta' \frac{v}{a}\right) \quad (2)$$

provides an accurate fit to all data points (black curves in Figure 4), with $\varepsilon' = 3.4640$ and $3.0196\ \mu m^{-1}$ and $\beta' = 1.9730$ and $3.0544\ \mu m^{-1}$ for HPS 59 and HPS 61. Thus the inversion of this equation predicts asphaltene amount deposited in the porous silica films by crude oil aging in terms of measured light absorbance.

Deposited amounts

For the full matrix of 18 brine conditions tested, the pairs of slide pieces for HPS 59 and HPS 61 after oil aging and post cleaning exhibit absorbance values at 365 nm lying within the range covered by the dry-phase calibrations, excepting the 3 samples with heaviest deposition. Thus equation 2 is generally applicable to the sample set to infer average values of volume *v* of dry asphaltene deposited in the porous film (across its entire thickness) per planar area *a*. Dividing the *v/a* ratio by the average film thickness and porosity for the two types (Table 1) gives the average percentage of pore volume occupied by asphaltene, with the results presented in Figure 5. Overall trends are quite similar to those for GSV in Figure 2, as expected from the correlation in the upper diagram of Figure 4, although inverted as increased GSV corresponds to decreased asphaltene amount. For HPS 59-templated pore frameworks aged in pure NaCl brine, asphaltene deposition is greatest at the lowest concentration, but relatively insensitive to concentrations above this. Proportional addition of calcium ions generally decreases deposition, particularly at high concentrations. For the first and last samples in the HPS 59 series the deposited amount decreases by almost an order of magnitude, from 7.1% to 0.75% of pore space filled with asphaltene. The HPS 61 samples largely mirror this behavior, although with an apparent step decrease for pure NaCl brines at around 100 mM and again with $CaCl_2$ hindering deposition to produce a monotonic decrease for the

mixed brines. Degassing apparently influences deposition, but without any systematic trend. To infer the average thickness of the asphaltene layer, assuming it uniformly lines all pore walls, the ratio *v/a* must be divided by the product of coat weight (Table 1) and specific surface area of the porous silica film. If the latter is estimated as 70 m^2/g, the two above-mentioned extremes for HPS 59 samples would correspond to average deposit thickness of 5.4 nm and 0.6 nm. Thus for the samples with least deposition, their asphaltene distribution may be patchy or only occupy part of the framework.

Spatial distribution of oil deposits

As UV-visible spectroscopy can only deduce an average deposit thickness in the porous silica films, FESEM is required to directly visualize their spatial distribution. Recall that Figure 1 displays the representative porous microstructures for HPS 59 and HPS 61 after pre-cleaning baths and plasma treatment. Analysis by FESEM verified that the silica frameworks remain intact and unaffected by brine-oil treatment and post-cleaning, and moreover that the larger-scale film cracks remain empty. Over the full central region of each slide piece sampled by scanning and spectroscopy the oil deposits are housed in the framework microstructure. Figure 6 displays constant magnification images of HPS 59 samples in a) the clean state, and after brine-oil treatments yielding asphaltene pore volume occupancies of b) 2.6%, c) 6.3% and d) 7.1% from spectroscopy. For the oil-treated samples the imaging brightness and contrast were controlled to focus only on the uppermost pore stratum. The residual deposits take the form of a nanometric layer lining the framework relatively uniformly, at least for this surface stratum, and the thickness of this lining increases in the same order as predicted by spectroscopy. With image analysis it may be feasible to extract the increase in planar projected area of the thickened framework to quantify the agreement with spectroscopy and determine whether this uppermost stratum is representative of framework interior deposition. Many oil treated slide pieces were browner over the approx. 2 mm bordering their bottom edge than throughout their central region. FESEM imaging revealed a scattering of submicron particulates adhering to the external framework surface in these lowest regions, which were completely absent from central regions. These particulates or flocs are presumably sedimented in the standing oil during aging.

DISCUSSION

For non-wetting oil encroaching on a solid substrate lined by a thin brine wetting film, at equilibrium the capillary pressure $P_c = P_o - P_w$ is balanced by the meniscus force $2\sigma J$, where σ and J are interfacial tension and mean curvature, and the disjoining pressure Π at the local film thickness h according to the augmented Young-Laplace equation [2,15]

$$P_c = 2\sigma J + \Pi(h) \quad (3)$$

Here J is positive or negative for concave or convex menisci, i.e. enclosing oil or brine. Thus for thin films hugging the substrate contours, this meniscus term acts to further thin the film if the substrate is curved towards itself (e.g. star-shaped pore) or thicken it if curving away from itself (e.g. spherical or cylindrical pore) [2,4], giving rise to the mixed wet-small (MWS) and mixed wet-large (MWL) subcategories, respectively.

In the current study the thick external brine film originally covering the microporous silica on oil immersion thins under gravitational drainage to a thin film sheathing the upper surface of the framework and spontaneously curving concavely into each brine-

filled pore opening. The surface pore throats can be viewed as toroidal pores (especially for HPS 59 – Figure 1), with hole radius 66 nm and body generating radius 10 nm, and the entire structure is an edge-shared network of these (actually puckered hexagonal rings). In the original water-wet state, the applied capillary pressure for oil to enter these toroidal holes is 1.5 MPa (from equation 3 with $\Pi = 0$, and assuming $\sigma = 50$ mN/m), i.e. vastly greater than any practical drainage P_c. However, for the convex thin film draped over the upper surface of the toroid, i.e. the cylindrical silica struts, the opposite applies; the meniscus term in equation 3 is -5.7 MPa. This is around two orders of magnitude greater than critical disjoining pressures inferred for metastable silicate-brine-crude oil thin films [15], thus rupturing the film to allow oil deposition on this toroid protruding upper surface. The meniscus recedes slightly and oil is free to continue deposition to cover the toroid and thus render oil-wet the entire upper stratum of the framework, causing spontaneous expulsion of the brine to expose the stratum below, and so on until the entire framework is oil-wet and oil-filled. For stable thin brine films, repelling over all thicknesses, it is an open question whether the brine can retain a few water molecule layers under this enormous pressure to hinder asphaltene/resin deposition.

Given this scenario, it is not surprising that all porous silica films in this study exhibit at least some deposition. Literature results [3,15] for thin films of NaCl brine between a smooth silicate substrate and a drop of crude oil similar to that used here display a transition from unstable to metastable to stable films as brine concentration increases over the range of our study and for our pH window 5.8-7. The trends in Figure 5 are qualitatively consistent with these findings, given that metastable and possibly even stable films will be ruptured by the silica framework curvature effects. The stabilizing influence of added calcium ions in Figure 5 may be due to it rendering both the silica-brine and brine-oil interfaces cationic, thus enhancing repulsion. Although the 72 h aging period was thought sufficient for frameworks of 5 μm thickness and high porosity to reach equilibrium, it is possible that the slow kinetics of polymer reconfiguration during deposition have not reached completion, and thus, e.g. added calcium merely slows deposition. It was envisaged that HPS 61 structures, giving a somewhat more closed-cell pore space compared to the strut-like HPS 59-type, may inhibit deposition as its solid framework curves less strongly towards itself. However from Figure 1 this difference is slight, as indeed is the reduction in deposition in Figure 5 for HPS 61.

CONCLUSION

The porous silica films are easy to prepare and provide a readily detectable response to crude oil deposition; a simple scanner suffices to distinguish differences. They may play a future role in rapid screening of wettability tendencies for brine-oil combinations, as a complement to contact angle measurements on impervious substrates. Furthermore, the frameworks show that fine pores in reservoirs can have a marked effect on wettability established during primary drainage, with structures curving predominately to enclose their micropores (e.g. an array of drilled microholes) enhancing water-wetness, while curvature towards the solid phase will favor the oil-wet state. Thus a distinction between mixed wet-large and mixed wet-small is required for both macropores and any micropores lining them to more completely categorize wettability. If an originally water-wet macropore bears a thin layer of water-wet silica framework considered here, it will display a stronger tendency to be oil-wet over the part of the pore wall contacted by oil on drainage, and also may propagate oil deposition via the underlying framework to expel brine residing in the macropore corners, irrespective of their size and shape.

ACKNOWLEDGEMENTS

Jouko Vyorykka and Pekka Salminen (Dow Chemical) are thanked for latex samples, as is Norman Morrow (University of Wyoming) for the Minnelusa crude oil sample and valuable discussions. Support from an ARC grant DP0881548 is also acknowledged.

REFERENCES

1. Salathiel, R.A., "Oil recovery by surface film drainage in mixed-wettability rocks", *J. Pet. Tech. Trans. AIME* (1973) **255**, 1216-1224.
2. Kovscek, A.R. et al., "A pore-level scenario for the development of mixed wettability in oil reservoirs", *AIChE J.* (1993) **39**(6), 1072-1085.
3. Morrow, N.R., "Wettability and its effect on oil recovery", *J. Pet. Tech.* (1990) **42**(12), 1476-1484.
4. Skauge, A. et al., "Experimental evidence of different intermediate wetting states", Proc. of the Soc. Core Analysts, Abu Dhabi, UAE, October 2004, Paper.
5. Anderson, W.G., "Wettability literature survey - Part 1: Rock/oil/brine interactions and the effects of core handling on wettability", *J. Pet. Tech.* (1986), 1125-1144.
6. Robin, M., "Interfacial phenomena: Reservoir wettability in oil recovery", *Oil & Gas Science and Technology – Rev. IFP* (2001) **56(1)**, 55-62.
7. Morrow, N.R., Mason, G., "Recovery of oil by spontaneous imbibition", *Curr. Opin. Colloid Interface Sci.* (2001) **6**, 321-337.
8. Lui, L., Buckley, J.S., "Alteration of wetting of mica surfaces", *J. Pet. Sci. Eng.* (1999) **24**, 75-83.
9. Lord, D.L., Buckley, J.S., "An AFM study of morphological features that affect wetting at crude oil-water-mica interfaces", *Colloids Surfaces A* (2002) **206**, 531-546.
10. Blunt, M.J., "Physically-based network modelling of multiphase flow in intermediate-wet porous media", *J. Pet. Sci. Eng.* (1998) **20**, 117-125.
11. Velev, O.D. et al., "Microstructured porous silica obtained via colloidal crystal templates", *Chem. Mater.* (1998) **10**, 3597-3602.
12. Carbajo, M.C. et al., "Macroporous silica and titania obtained using polystyrene-hydroxyethyl methacrylate as template, *J. Mater. Chem.* (2002) **12**, 2740-2746.
13. Alcantar, N. A. et al., "Effect of water plasma on silica surfaces: Synthesis, characterization and applications", Royal Society of Chemistry Special Publications (1999), 235, 212-222.
14. Marczewski, A.W., Szymula, M., "Adsorption of asphaltenes from toluene on mineral surface", *Colloids Surfaces A* (2002) **208**, 259-266.
15. Basu, S., Sharma, M.M., "Measurement of critical disjoining pressure for dewetting of solid surfaces", *J. Colloid Interface Sci.* (1996) **181**, 443-455.

Table 1. Mean and standard deviation of gravimetrically determined coat weight of the films for the two latex types, before and after calcination, the ratio of these, and the inferred coat thickness and porosity.

Latex	Coat weight uncalcined [g/m^2]	Coat weight calcined [g/m^2]	Mass ratio calcined/ uncalcined	Thickness [μm]	Porosity [%]
HPS 59	5.91 ± 0.61	0.94 ± 0.13	0.158 ± 0.014	5.37 ± 0.55	92.1 ± 0.7
HPS 61	6.24 ± 0.75	0.78 ± 0.14	0.125 ± 0.015	5.67 ± 0.68	93.8 ± 0.8

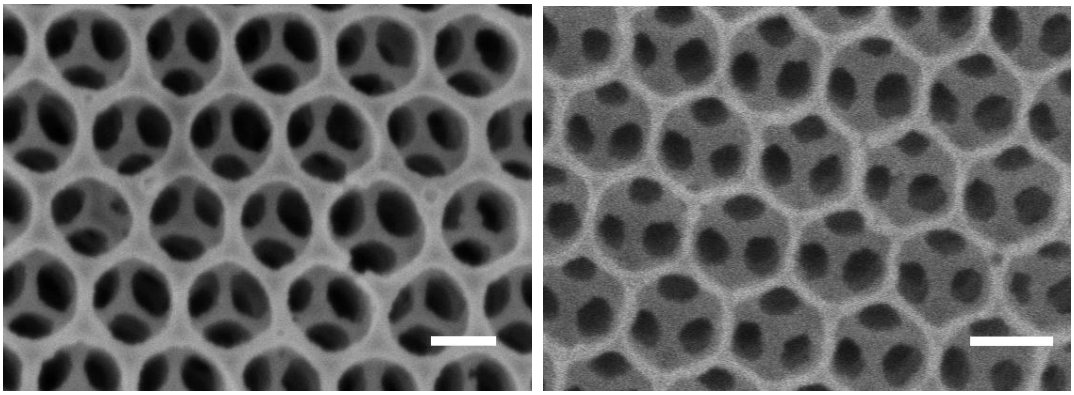

Figure 1. Representative FESEM images looking down on the clean porous silica films templated by the HPS 59 (at left) and 61 (right) latexes, with scale bar equal to 100 nm in both cases.

	HPS 59				HPS 61			
	Na	Na degas	NaCa	NaCa degas	Na	Na degas	NaCa	NaCa degas
16 mM	166.3		177.3		218.6		188.8	
32 mM	188.5		184.6		206.5		202.2	
64 mM	184.6		204.9		202.1		212.6	
128 mM	194.8	193.3	190.7	197.2	202.4	189.8	219.8	224.8
268 mM	194.7	188.0	206.2	229.7	210.2	194.1	240.6	230.6
612 mM	196.0	190.0	227.2	243.8	207.7	188.4	241.9	245.5

Figure 2. Cropped scanned images of the silica framework-coated slide pieces of the two latex types (HPS 59 and HPS 61) after oil treatment and post-cleaning, for the full matrix of brines, i.e. 6 varying NaCl concentrations (rows) and with degassing and/or addition of 10% (mol/mol) $CaCl_2$ (for columns labeled NaCa). The corresponding number is the average gray scale value of the image.

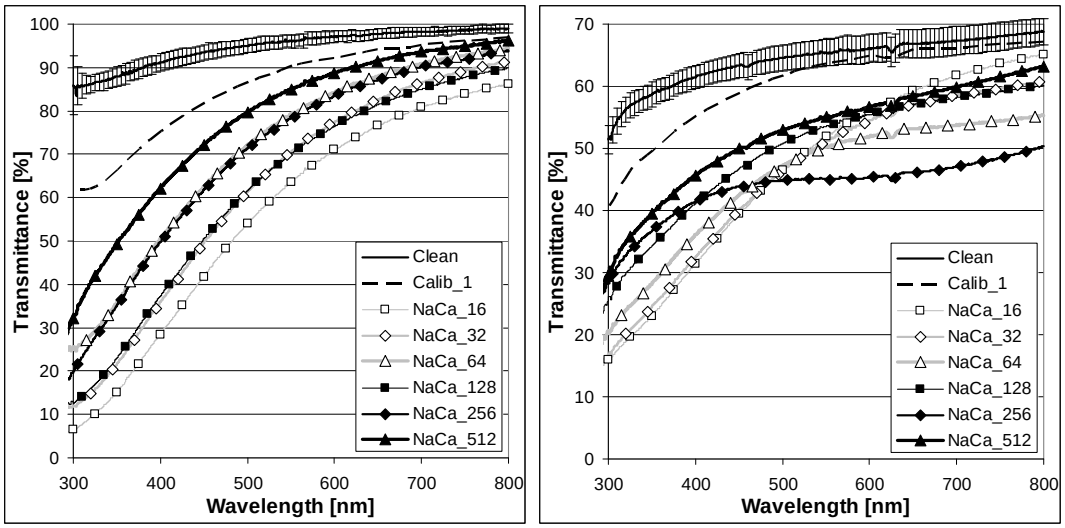

Figure 3. UV-visible transmission spectra of the porous silica film-coated slides of the HPS 59 (at left) and HPS 61 (right) types for a clean sample (showing error bars), its first dry-phase calibration standard, or after oil treatment and post-cleaning for the 6 concentrations of calcium-containing brines (NaCa).

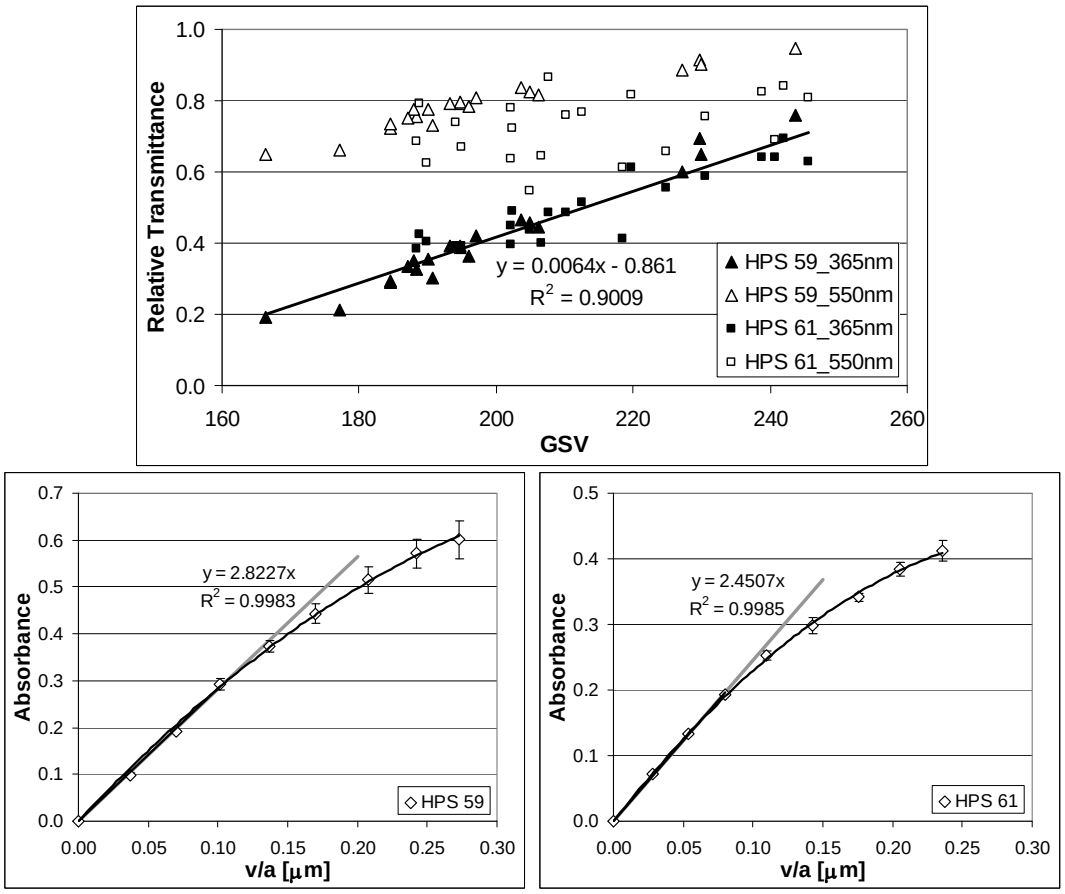

Figure 4. Upper diagram compares gray scale value from scanning and relative transmittance (at the two wavelengths) from spectroscopy for the matrix of samples. Lower plots are dry-phase calibration curves for volume per planar area of asphaltene deposit in the HPS 59 (at left) and HPS 61 (right) frameworks.

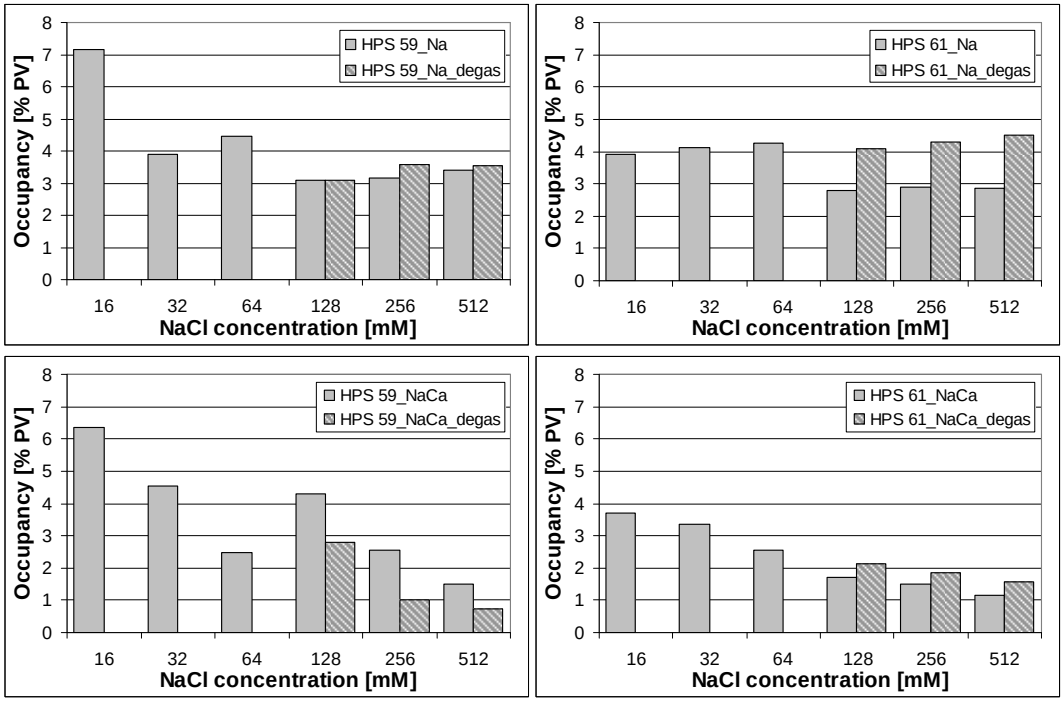

Figure 5. Percentage of HPS 59 (left column) and HPS 61 (right) framework film pore volume occupied by asphaltene deposits after oil aging and post-cleaning versus NaCl concentration in the brine, without (upper pair) or with (lower) added calcium chloride, including effect of brine degassing (hatched bars).

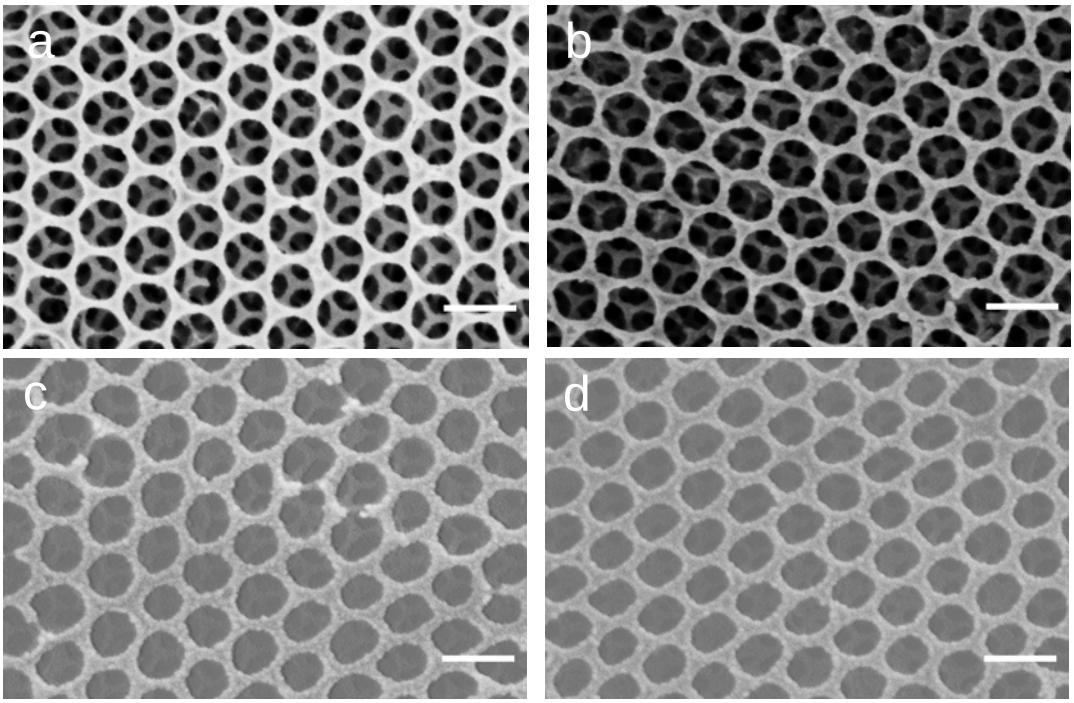

Figure 6. Representative FESEM images of the surface of HPS 59-templated porous silica films a) clean, and after oil aging and post-cleaning for the brines b) 256 mM NaCl + 25.6 mM $CaCl_2$, c) 16 mM NaCl + 1.6 mM $CaCl_2$, and d) 16 mM NaCl without $CaCl_2$. Scale bar is 200 nm in all cases.